

## Ⓔ **Avalanche Fatalities during Atmospheric River Events in the Western United States**

BENJAMIN J. HATCHETT,<sup>a</sup> SUSAN BURAK,<sup>b</sup> JONATHAN J. RUTZ,<sup>c,d</sup> NINA S. OAKLEY,<sup>a,d</sup>  
EDWARD H. BAIR,<sup>e</sup> AND MICHAEL L. KAPLAN<sup>a</sup>

<sup>a</sup> *Division of Atmospheric Science, Desert Research Institute, Reno, Nevada*

<sup>b</sup> *Snow Survey Associates, Bishop, California*

<sup>c</sup> *Western Region Headquarters, National Weather Service, Salt Lake City, Utah*

<sup>d</sup> *Center for Western Weather and Water Extremes, Scripps Institution of Oceanography, University of California, San Diego, La Jolla, California*

<sup>e</sup> *Earth Research Institute, University of California, Santa Barbara, Santa Barbara, California*

(Manuscript received 12 September 2016, in final form 5 February 2017)

### ABSTRACT


The occurrence of atmospheric rivers (ARs) in association with avalanche fatalities is evaluated in the conterminous western United States between 1998 and 2014 using archived avalanche reports, atmospheric reanalysis products, an existing AR catalog, and weather station observations. AR conditions were present during or preceding 105 unique avalanche incidents resulting in 123 fatalities, thus comprising 31% of western U.S. avalanche fatalities. Coastal snow avalanche climates had the highest percentage of avalanche fatalities coinciding with AR conditions (31%–65%), followed by intermountain (25%–46%) and continental snow avalanche climates (<25%). Ratios of avalanche deaths during AR conditions to total AR days increased with distance from the coast. Frequent heavy to extreme precipitation (85th–99th percentile) during ARs favored critical snowpack loading rates with mean snow water equivalent increases of 46 mm. Results demonstrate that there exists regional consistency between snow avalanche climates, derived AR contributions to cool season precipitation, and percentages of avalanche fatalities during ARs. The intensity of water vapor transport and topographic corridors favoring inland water vapor transport may be used to help identify periods of increased avalanche hazard in intermountain and continental snow avalanche climates prior to AR landfall. Several recently developed AR forecast tools applicable to avalanche forecasting are highlighted.

## 1. Introduction

In mountain environments of the conterminous western United States (wUS), snow avalanches are a dangerous type of mass movement that pose significant hazards to life and property, yielding millions of dollars per year in economic losses (National Research Council 1990; Mock and Birkeland 2000). Since 1995, avalanches have caused an

average of 28 deaths per year in the United States (Colorado Avalanche Information Center 2015). Slab avalanches are the most dangerous type of avalanche and result when a failure initiates and propagates outward in a weak layer underlying a cohesive slab of snow, causing the slab to become unsupported (Schweizer et al. 2003). Fatal slab avalanches are commonly triggered by human actions but also occur because of natural release mechanisms resulting from loading by newly fallen or wind-deposited snow. Forecasting slab avalanche occurrence is a major challenge because of the complex interactions among terrain, snowpack, and meteorology (LaChapelle 1980; Schweizer et al. 2003, 2008). Furthermore, avalanches are not always weather related and by nature are multivariate problems (Mock and Birkeland 2000).

Prior studies on the synoptic conditions resulting in large avalanches showed the presence of an upstream 500-hPa trough (Mock and Birkeland 2000; Birkeland

 Denotes content that is immediately available upon publication as open access.

 Supplemental information related to this paper is available at the Journals Online website: <http://dx.doi.org/10.1175/JHM-D-16-0219.s1>.

Corresponding author e-mail: Benjamin J. Hatchett, benjamin.hatchett@gmail.com

DOI: 10.1175/JHM-D-16-0219.1

© 2017 American Meteorological Society. For information regarding reuse of this content and general copyright information, consult the AMS Copyright Policy ([www.ametsoc.org/PUBSReuseLicenses](http://www.ametsoc.org/PUBSReuseLicenses)).

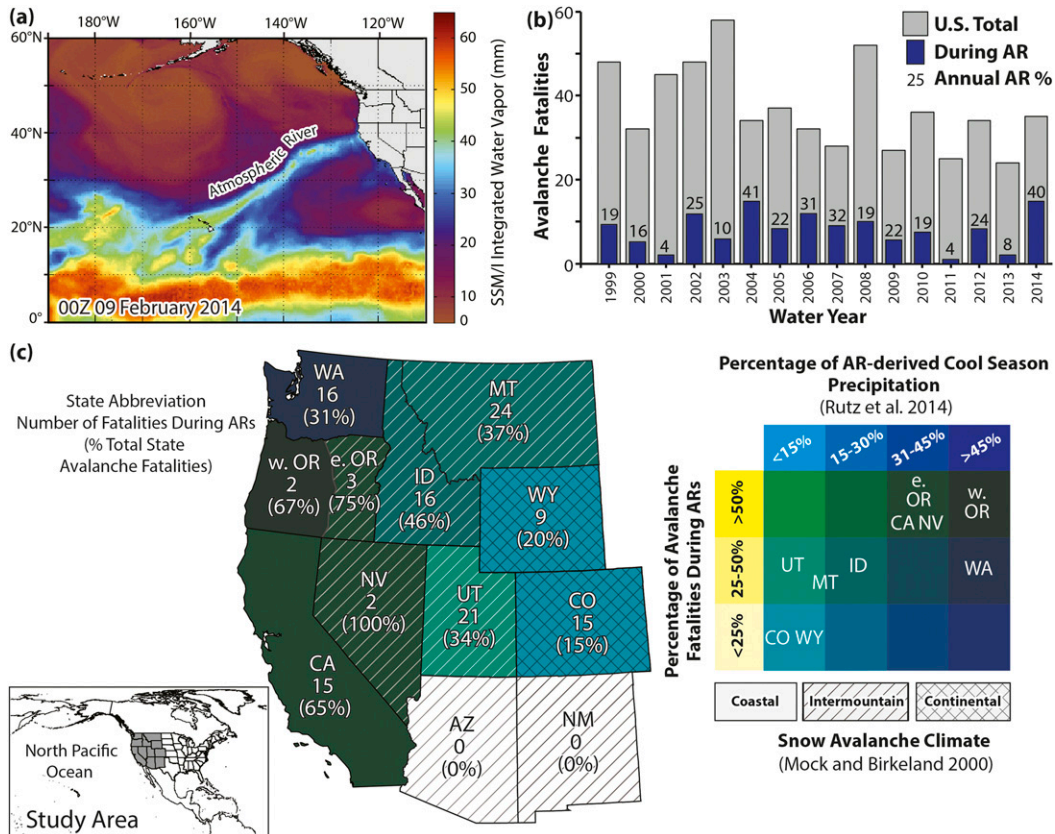


FIG. 1. (a) Example AR along the wUS identified using SSM/I satellite-derived IWV (filled colors). (b) Total U.S. avalanche fatalities by water year (gray bars) and fatalities linked to AR conditions in the wUS (blue bars). Annual percentages of wUS fatalities associated with ARs are listed as a percent of total U.S. fatalities. (c) Choropleth map of the wUS where colors are created from blending the percentage of AR-derived cool season precipitation in blues (Rutz et al. 2014) and the percentage of avalanche fatalities during AR events in yellows. The Mock and Birkeland (2000) snow climates are represented by overlain cross hatches (continental), single hatches (intermountain), or no hatches (coastal).

et al. 2001), although other synoptic patterns can lead to avalanches (Esteban et al. 2005; Muntán et al. 2009). Here we focus on atmospheric conditions characterized by narrow plumes of concentrated water vapor flux called atmospheric rivers (ARs; Zhu and Newell 1998; Ralph et al. 2004). ARs originate as a combination of local convergence along the warm conveyor belt and cold frontal region of the extratropical cyclone and as direct poleward transport of tropical moisture (Bao et al. 2006). ARs are often identified via satellite as elongated regions of enhanced column-integrated water vapor (IWV; Fig. 1a) and have important roles in wUS hydrometeorology. They frequently contribute to cool season (defined as November–April) extreme precipitation and flooding events (Ralph et al. 2006; Dettinger et al. 2011; Alexander et al. 2015; Swales et al. 2016) and supply large percentages of climatological precipitation (Rutz et al. 2014), with mean largest 72-h events often contributing 10%–25% of total snow water

equivalent (SWE; Serreze et al. 2001). While studies linking ARs to avalanches do exist (Hansen and Underwood 2012), they are limited to a few regions and a small number of case studies. Anecdotal evidence exists for a linkage between ARs and avalanches and is used by avalanche forecast centers and the public, but this connection has not yet been fully documented in detail. Here we attempt to quantify the linkage between ARs and deadly avalanches using readily available and archived data.

We hypothesize that since ARs are associated with extreme cool season precipitation, they should contribute to avalanches by favoring snowfall in excess of the 30-cm storm total threshold required for avalanche activity established by Atwater (1954) and supported by Bair (2013) and Perla (1970). To address this hypothesis, we illustrate the relationships between AR conditions and avalanche fatalities throughout the wUS and place this information into the context of established snow

avalanche climate and hydroclimate regimes. We demonstrate the importance of recently identified preferential pathways for inland moisture transport (Rutz et al. 2015; Swales et al. 2016) and show how integrated water vapor transport can be used as a tool to identify magnitudes of precipitation and the extent of inland penetration. We then demonstrate that heavy to extreme precipitation and rapid snow loading in excess of commonly used thresholds for avalanche activity occurred during a large fraction of the avalanche fatalities coinciding with AR conditions. Finally, we highlight several recently developed AR forecast tools that can be used by avalanche forecasters, emergency managers, and the general public. These tools can be used to more precisely predict timing, location, and inland penetration of ARs.

## 2. Data

Archived avalanche incidents in the wUS between November 1998 and April 2014 were acquired from Atkins (2007) and the Colorado Avalanche Information Center (2015). Because of a lack of archived nonfatal avalanche observations, we were unable to quantify the frequency of nonfatal avalanches during AR events in a meaningful manner. Atmospheric fields of 500-hPa geopotential height, 700-hPa air temperature, meridional and zonal wind, and specific humidity on isobaric surfaces were derived from daily 32-km horizontal resolution North American Regional Reanalysis (NARR) output (Mesinger et al. 2006). Daily values of precipitation and SWE were acquired from 335 Snowpack Telemetry (SNOTEL) stations (<https://www.wcc.nrcs.usda.gov/snow/>) in the wUS spanning from 1 November 1979 to 30 April 2014. SNOTEL data were quality controlled following Meek and Hatfield (1994) and Raleigh and Lundquist (2012). Values were set to missing when negative precipitation or SWE values were observed. For precipitation, we allowed a maximum daily value of 150 mm and a 150 mm day<sup>-1</sup> rate-of-change limit to detect spurious jumps in data. For SWE, we used a similar maximum daily value of 150 mm of SWE change and a 300 mm day<sup>-1</sup> rate-of-change limit. Estimates of cool season climatological AR contributions to precipitation, or AR precipitation percentages, came from Rutz et al. (2014). These percentages varied in space by state and thus we present binned values (<15%, 15%–30%, 31%–45%, and >45%). We used the regional snow avalanche climates identified by Mock and Birkeland (2000) to contextualize how avalanche fatalities during AR events related to different snow avalanche climates. These climates are based on well-established thresholds and ranges of seasonal snowpack

variables including temperature, snowfall, SWE, rainfall, and December snowpack vertical temperature gradient. Large snowpack temperature gradients contribute to the formation of weak layers in intermountain and continental climate snowpacks and lead to subsequent deep slab avalanches (Schweizer et al. 2003; Marienthal et al. 2015). In coastal climates, avalanches often result from failures occurring within storm snow layers or at the old–new snow interface (Bair 2013).

## 3. Methods

The latitude and longitude of each avalanche incident was estimated from archived avalanche reports. SNOTEL observations from stations located within a 0.5° radius of each incident (eight stations on average) were used to calculate the precipitation percentiles from the period of record (typically 1981–2014) nonzero cool season precipitation days. We compared these values with the maximum daily precipitation percentiles observed between 4 days prior to the avalanche event day and 1 day after. This period covers complete storm event precipitation at time scales relevant for avalanche hazard. Changes in SWE (hereafter  $\Delta$ SWE) were calculated as the difference in SWE over this 6-day period to quantify total new snow loading. We also calculated the greatest 1- and 2-day change in SWE over the 6-day window to estimate the maximum rates of new snow loading, as slow loading can strengthen snow while rapid loading weakens snowpack strength (Narita 1980; McClung 1981; Schweizer et al. 2003).

We used NARR products to identify AR conditions. We calculated integrated vapor transport (IVT) and integrated water vapor (IWV) following Zhu and Newell (1998) from 1000 to 300 hPa. Our AR criteria requires the presence of  $IVT > 250 \text{ kg m}^{-1} \text{ s}^{-1}$  (Rutz et al. 2014) within 250 km upstream of the incident location at any time up to 4 days prior to the incident for the event to be associated with an AR. Events near our daily threshold were checked against 3-hourly NARR output. We corroborated ARs identified in NARR with an AR catalog developed following Rutz et al. (2014), who defined AR conditions using the same IVT threshold and occurring for at least one 6-h time period. This catalog used the 2.5° horizontal resolution National Centers for Environmental Prediction–National Center for Atmospheric Research (NCEP–NCAR) reanalyses (Kalnay et al. 1996) instead of the 1.5° ERA-Interim used in the study of Rutz et al. (2014). We used this catalog to count the number of cool season AR days over the study period. The total number of fatalities counted during AR conditions was then divided by the total number of AR days in a 2° × 3° [longitude by

latitude; see Fig. 3a (described in greater detail below for examples] box upstream of each state to yield an estimate of AR avalanche deaths per AR. A larger  $2^{\circ} \times 4^{\circ}$  box was used for Utah and Colorado in order to capture both northerly and southerly transport pathways (Rutz et al. 2015). Composite analysis, also known as superposed epoch analysis when performed on time series (e.g., Mass and Portman 1989; Joseph et al. 1994), was performed on IVT and geopotential height fields 2 days prior to avalanche events by state to identify signals relevant to mountain weather and avalanche forecasts. The primary signals of interest included magnitudes of IVT and preferential corridors of inland moisture transport (Alexander et al. 2015; Rutz et al. 2015; Swales et al. 2016).

When sufficient information about the avalanche incident was available in the archived reports, it was used to verify that an incident resulted from snowpack instability produced by recent precipitation. Incidents that were clearly unrelated to recent snowfall were excluded. We did not differentiate between failures that occurred within the storm snow or on persistent weak layers. In three retained cases, AR conditions were present more than 4 days prior to the incident but resulted in the most recent snowfall and linked to the incident via the report. Three other cases were also included that had no fatalities but involved notable near misses. In evaluating avalanche fatalities, the importance of human decision-making and avalanche occurrence cannot be overlooked (Fredston and Fesler 2011; McClung 2002). As the archived incident reports contained insufficient information to perform a robust quantitative social analysis of human factors involved, we proceed under the assumption that human avalanche triggering is relatively constant between AR and non-AR storms.

## 4. Results and discussion

### a. Fatalities and ARs

AR conditions were present during 105 avalanche incidents resulting in 123 fatalities between 1998 and 2014, comprising 21% of the U.S. avalanche fatalities and 31% of wUS fatalities. A table of incidents is provided in the supplemental material. The number of avalanche fatalities occurring during ARs (hereafter AR fatality percentages) varied by year from 1 to 14 and accounted for 4%–41% of the U.S. annual total (Fig. 1b). The most AR fatalities occurred during water years 2002, 2004, and 2014 (Fig. 1b). The avalanche cycle of 10–13 March 2002 resulted in seven deaths in four states (Figs. 2a–c). The 9–18 February 2014

(Figs. 2d–f) cycle resulted in 10 deaths in five states and was associated with a progressive series of three land-falling ARs between 27 January and 15 February 2014. The choropleth map (Fig. 1c) utilizes blended colors based upon the AR precipitation percentages estimated by Rutz et al. (2014) and our calculated AR fatality percentages.

We find broad agreement between AR precipitation percentages, snow avalanche climates, and AR fatality percentages (Fig. 1c). These results are consistent with Mock and Birkeland (2000) because coastal (continental) snow avalanche climates have greater (lesser) annual snowfalls and have higher (lower) AR percentages (Rutz et al. 2014). Coastal snow avalanche climates such as California and western Oregon have high AR fatality percentages (65% and 67%, respectively) and high AR precipitation percentages (>31%). Eastern Oregon and Nevada are characterized by intermountain snow avalanche climates but have large AR precipitation percentages (31%–45%). All deaths in Nevada and eastern Oregon occurred during ARs; however, the sample size is small (five). Washington is an outlier with 31% AR fatalities, despite being in the largest bin of AR precipitation percentages (>45%) and having a similar number of fatalities compared to California. This finding presumably results from frequent avalanche deaths on Mount Rainier during the spring mountaineering season. Lower AR precipitation percentages are observed in the intermountain snow avalanche climates of Idaho (15%–30%), Montana (15%–30%), and Utah (>15%) with a corresponding decrease in AR fatality percentages (46%, 37%, and 34%, respectively) compared to coastal snow avalanche climates. The pattern of decreasing fatalities and precipitation percentages with increasing distance inland extends into the continental snow avalanche climates. We find the lowest AR fatality percentages in Wyoming (20%) and Colorado (15%). Arizona and New Mexico had no reported fatalities during the period studied.

Although the frequency of AR events diminishes as one moves inland (Rutz et al. 2014; Swales et al. 2016), the relative frequency of fatal avalanches during AR conditions tends to be small, similar to flood case studies (e.g., Ralph et al. 2006; Dettinger et al. 2011). The number of cool season AR days shows a marked decrease in average AR day frequency as one moves inland regardless of chosen latitude (Fig. 3a). However, the number of fatalities during ARs and the ratio of avalanche deaths during AR conditions to total AR days does not decrease in a similar manner (Fig. 3b). The ratio of 0.02–0.03 fatalities per AR day in Washington and California, respectively, increases to 0.16–0.22 in Utah and Colorado. Although ratios are lower in Idaho



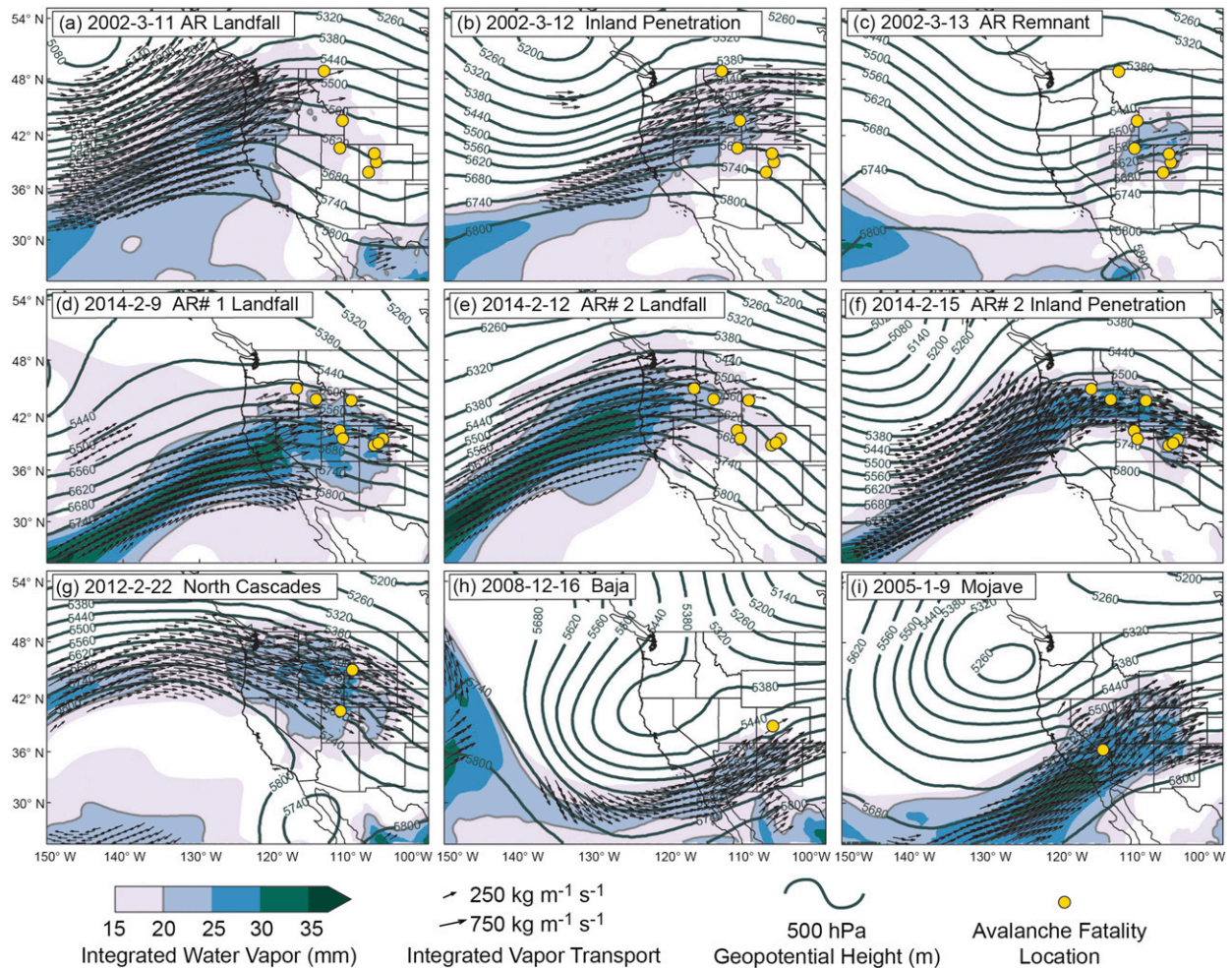


FIG. 2. Examples of daily mean atmospheric conditions during AR events that coincided with widespread avalanche deaths in multiple states during (a)–(c) 11–13 Mar 2002 and (d)–(f) 9–15 Feb 2014. (h)–(j) Examples for three other primary inland pathways described in Rutz et al. (2014).

(0.06) and Montana (0.09), fatalities during AR conditions compose larger percentages of total avalanche fatalities than the farther inland states (Fig. 2c). This suggests that although their presence is less frequent in inland locations, ARs have relatively more important roles in intermountain and continental regions where snowpacks are characteristically weaker. It also implies that if an AR is forecast to occur near or directly over a region, increased situational awareness should arise with avalanche forecasters and others such as emergency managers who may be required to respond to avalanche incidents, particularly in inland locations. Under forecast AR conditions, avalanche forecasters should assess the capability of the snowpack to handle a loading event that may be realized as an intense and/or long-duration precipitation event with substantial increases in SWE (see sections 4d and 4f) and high-frequency variations in hydrometeor characteristics (Bair et al. 2012). This may include detailed evaluations of

existing snowpack stability via vertical variation in snowpack grain size and hardness (Schweizer and Jamieson 2003), monitoring of hydrometeors throughout storms (Bair et al. 2012) and through identification of the presence of persistent weak layers, which were noted by Schweizer and Jamieson (2001) as being involved in 70% of 186 skier-triggered avalanches. This approach is analogous to flood forecasting. Antecedent land surface conditions such as soil moisture can strongly control runoff and streamflow during precipitation events (e.g., Leung and Qian 2009; Ralph et al. 2013a), but one must also consider the precipitation intensity–duration relationships during observed storms (e.g., Doswell et al. 1996; Ralph et al. 2013a) in order to provide an accurate forecast of flood hazard.

#### b. Synoptic setup during ARs

Examples of characteristic atmospheric conditions during fatalities are shown in Fig. 2. Figures 2a–c show

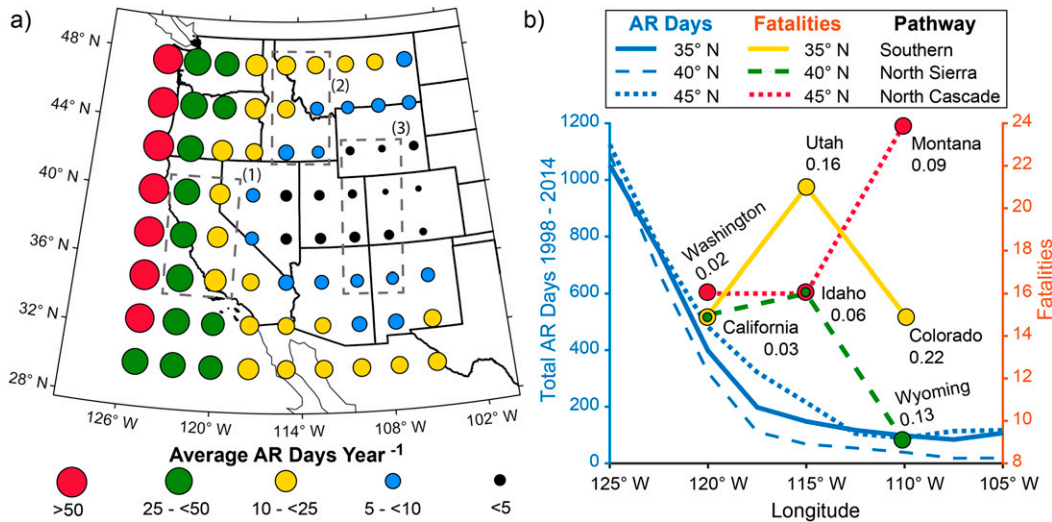


FIG. 3. (a) Average number of cool season AR days per year for grid points in the AR catalog generated following Rutz et al. (2014) but for the NCEP–NCAR reanalyses product. Dashed gray boxes indicate examples of the sets of grid points used to calculate the ratios of fatalities during AR days to total AR days in each state shown in (b). Box 1 was used in California, box 2 for Montana, and box 3 for Colorado. (b) Left y axis shows the total AR days between 1998 and 2014 for three primary pathways (35°, 40°, 45°N) as a function of longitude along each grid point. Right y axis shows the number of avalanche fatalities during AR conditions for states with more than 10 fatalities. Numbers denote the ratio of avalanche fatalities during AR conditions to total numbers of AR days.

the March 2002 AR event and Figs. 2d–f exhibit two ARs during February 2014. All are AR events, although the moisture transport conditions vary from massive transport regimes (Fig. 2a) to narrow and filamentary plumes (Fig. 2d). The vast majority of individual cases (not shown) demonstrated canonical AR conditions of strong IVT and extended IWV plumes. The 500-hPa geopotential heights show that while many atmospheric patterns can be associated with AR conditions, most include an upstream trough over the northeastern Pacific (Birkeland et al. 2001; Muntán et al. 2009) consistent with the findings of Mundhenk et al. (2016) that AR activity increases in the wUS when a negative height anomaly or trough exists in the northeastern Pacific (see also Fig. 4). Examples include a deep trough (Fig. 2a), a shortwave trough (Fig. 2c), a ridge (Figs. 2d,h), amplified meridional flow with downstream blocking (Fig. 2e), and a closed low (Fig. 2g).

### c. Possible causes of widespread avalanche cycles

Incident reports and observations archived by avalanche centers in intermountain and continental climates indicated shallow snowpacks that formed after early season snowfalls were weakened by basal and near-surface faceting during subsequent multiple weeks of cold and dry weather [see also Mock and Birkeland (2000)]. Deadly avalanche cycles occurred when the arrival of AR conditions produced heavy precipitation and rapid loading of existing weak snowpacks. These

conditions were involved in the aforementioned 14–17 March 2002 (Figs. 2a–c) and the 9–18 February 2014 avalanche cycles (Figs. 2d–f). Both avalanche cycles resulted in widespread fatalities between intermountain states such as Colorado, Idaho, Montana, and Utah and elevated avalanche hazards throughout most wUS mountain areas.

During 14–17 March 2002, the Utah Avalanche Center (<http://www.utahavalanchecenter.org>) forecast high avalanche hazard and noted a weak and shallow pre-existing snowpack with deep slab instability that led to large and dangerous avalanches. An avalanche forecaster reported triggering a large avalanche that failed on a weak layer formed 2 months prior. No other archived information from avalanche centers could be found for this avalanche cycle. During the 9–18 February case, extreme avalanche hazard was forecast by the Utah Avalanche Center with extensive natural avalanche activity occurring at elevations ranging from 1800 to 3400 m throughout their forecast region. Forecasters noted the widespread existence of persistent slabs and a weak snowpack that could fail to the ground surface once failure was initiated. Leading up to this avalanche cycle, a snowpack summary written on 30 January 2014 by the Bridger Teton Avalanche Center (<http://www.jhavalanche.org>) noted that the snowpack had poor (weak) structure, with prior summaries indicating frequent dry and cold conditions during November–January. During 7–20 February, they wrote that



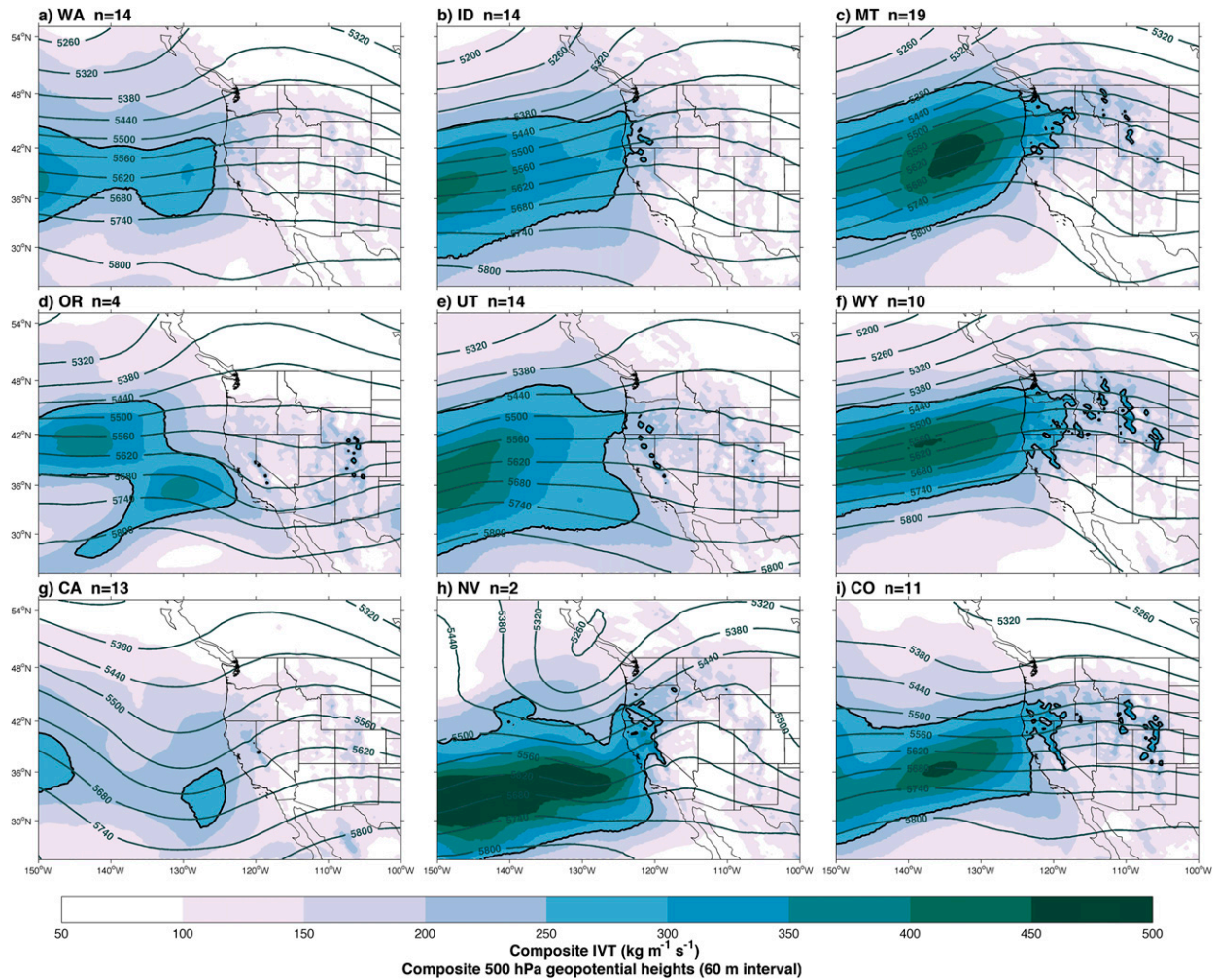


FIG. 4. Daily composites of IVT ( $\text{kg m}^{-1} \text{s}^{-1}$ ; filled colors; black outline shows the  $250 \text{ kg m}^{-1} \text{s}^{-1}$  contour) and 500-hPa heights (gray contours) for each state [(a) Washington, (b) Idaho, (c) Montana, (d) Oregon, (e) Utah, (f) Wyoming, (g) California, (h) Nevada, and (i) Colorado] for the period 2 days before avalanche fatalities during ARs occurred. The number of unique fatality days for each composite is indicated by  $n$  in the figure labels.

westerly flow brought abundant moisture, mild temperatures, and widespread natural- and human-caused avalanches. Accident reports written by the Northwest Avalanche Center (<http://www.nwac.us>) regarding fatalities mentioned failures occurring on melt-freeze crusts formed by the anomalously warm and dry January and the existence of a shallow, weak, continental-type snowpack with varying weak layers of crusts and facets. These scenarios provide evidence for the plausible mechanism of how a short-term, high-impact weather event such as an AR can lead to widespread avalanche hazard and fatalities, provided ongoing longer-term hydroclimate conditions have favored the establishment of shallow and weak snowpacks.

These situations have relevance for the future of avalanche forecasting and hazard. Projections from the

CMIP5 ensemble for the mid- to late twenty-first century in the wUS suggest reduced mean snow depths (Krasting et al. 2013) with increased frequencies of dry days (Polade et al. 2014). They also project increases in AR intensity and extreme precipitation (Lavers et al. 2015). We interpret the projections as supporting increased durations between storms where weakening of climatologically shallower snowpacks occurs as a result of faceting processes produced by strong vapor pressure gradients (Blackford 2007). Rapid loading of weak snowpacks by extreme precipitation events promotes widespread snowpack instability (Schweizer et al. 2003). Furthermore, as observed snowpack losses due to ablation occur most frequently late in the cool season (March–April; Kapnick and Hall 2012), large late season storms may lead to decreased snow stability during a

time of year previously characterized by increased stability. With increasing numbers of recreational backcountry users and changing mountain snowpack conditions, we might expect the future to be characterized by enhanced exposure to avalanche hazard throughout the wUS.

#### *d. Inland penetration of ARs*

An important aspect of the identified relationship between AR percentages, snow avalanche climate, and AR fatalities is the mechanism through which moisture can be transported into the interior wUS. Alexander et al. (2015) and Rutz et al. (2015) showed that the most common pathways of moisture penetration into the interior wUS are gaps or corridors of relatively low topography in the western cordillera. These include the southern Cascades (Figs. 2a,b), gaps in the Sierra Nevada (Fig. 2d), lower topography in the northern Cascades (Fig. 2h), through Baja California (Fig. 2i), and across the Mojave Desert (Fig. 2j). While these patterns are not ubiquitous, they occur frequently enough to be noted as a possible forecasting aide by allowing forecasters to identify the potential of moisture transport through a terrain gap and subsequent anomalous enhancements in downstream precipitation. Composite analysis of IVT 2 days prior to events (Fig. 4) hints at the importance of inland pathways, particularly through the northern Cascades (Figs. 4c,d) and north of the Sierra Nevada (Figs. 4b,i). Our composite results agree with the findings of Rutz et al. (2015), who showed that farther inland-penetrating events are characterized by stronger offshore transport (Figs. 4c,f,i) compared to coastally focused events (Figs. 4a,d,g). The northern Cascades pathway is consistent with the findings of Birkeland and Mock (1996), who suggested that lower-elevation upstream terrain allowed moisture to be transported into the Bridger Mountains of Montana. Swales et al. (2016) used self-organizing maps to show that the magnitude of IVT (Fig. 4) could be a useful tool in relating localized extreme precipitation to larger-scale synoptic conditions in agreement with Rutz et al. (2015). Our composite analyses also agree with the findings of Swales et al. (2016), who showed that the presence of a stationary ridge over the southwestern United States produces a favorable synoptic setup for activation of the northerly inland transport pattern into Idaho, Montana, and Wyoming (Figs. 4b,c,f). This would imply that looking farther upstream into the Gulf of Alaska for the presence of a deep trough (Mock and Birkeland 2000; Birkeland et al. 2001) is important to correctly identify this northerly pathway. The complexity of wUS terrain presents difficulties for numerical precipitation forecasts, and incorporating analyses of

moisture transport can offer improvements in extreme precipitation forecasts at longer lead times than numerical weather model-derived quantitative precipitation forecasts (Lavers et al. 2014, 2016). Our findings suggest that IVT can be applied to improve forecasts of increased avalanche hazard by identifying likelihoods of inland penetration and subsequent extreme precipitation.

#### *e. Potential applications of IVT tools in avalanche forecasting*

Newly developed IVT forecast tools (Fig. 5; Cordeira et al. 2017) may provide useful additional guidance to mountain weather and avalanche forecasters as well as emergency managers and the general public. These tools have been developed for the NCEP Global Ensemble Forecast System (GEFS) and provide forecasters with a probabilistic perspective to identify and track ARs in the northeastern Pacific. They allow specific attention to be paid to the structure, intensity, and orientation during landfall along the wUS coast (Cordeira et al. 2017). This is of particular importance in identifying preferential inland pathways (Rutz et al. 2015) and favorable relationships with topography, allowing for copious precipitation to result (Ralph et al. 2013a). The tools can be used by forecasters in an ingredients-based approach (Doswell et al. 1996), where multiple forecast tools and antecedent snowpack conditions can be evaluated in concert to address whether avalanches during AR conditions are possible and/or plausible under given scenarios.

Here we focus on the 48-h forecast initialized at 1200 UTC 8 December 2016. Figures 5a and 5b demonstrate IVT magnitudes in plan view following the convention that only IVT vectors above the AR threshold of  $250 \text{ kg m}^{-1} \text{ s}^{-1}$  are shown. The probability of IVT magnitudes in exceedance of this threshold, based upon the 20 member GEFS, is shown in Fig. 5a. Probabilities are calculated as the fraction of ensemble members with IVT magnitudes in exceedance of the  $250 \text{ kg m}^{-1} \text{ s}^{-1}$  threshold. The transport of moisture through the northern Sierra pathway (Rutz et al. 2015; Alexander et al. 2015) and inland into the Intermountain West are clearly shown (Figs. 5a,b). A time-latitude plot (Fig. 5c), initialized at 0600 UTC 8 December, highlights the likelihood over a 10-day forecast horizon that a given point along the wUS coast will have AR conditions present. This tool can also be used to note the meridional migration of an AR along the coast. As ARs migrate along the coast (typically from north to south), multiple inland pathways can allow moisture to penetrate inland, while a stationary AR may or may not favor inland moisture transport. This tool allows forecasters to assess model forecast consistency and the likelihood that their region of interest may experience AR



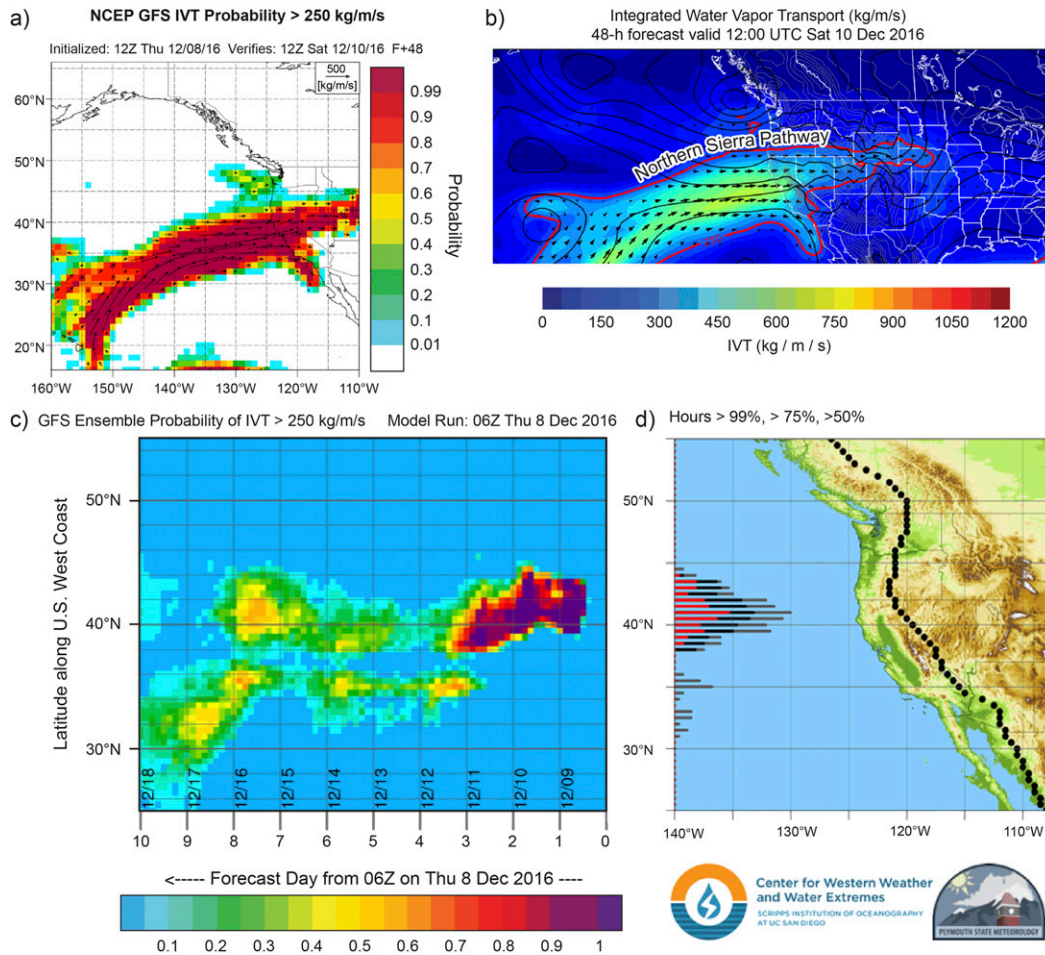


FIG. 5. Forecast tools that can be used in evaluating AR and moisture transport characteristics with regards to avalanche hazard in the wUS. The event shown penetrated inland via the northern Sierra pathway (Rutz et al. 2015; Alexander et al. 2015). (a) Filled contours show the probability of IVT magnitudes exceeding AR criteria (>250 kg m<sup>-1</sup> s<sup>-1</sup>) based upon 20 members of the NCEP GEFS for the 48-h forecast valid at 1200 UTC 10 Dec 2016. Vectors show IVT from the control forecast. (b) NOAA Western Regional Headquarters GEFS 48-h IVT forecast valid at 1200 UTC 10 Dec 2016. Magnitudes of IVT are shaded (kg m<sup>-1</sup> s<sup>-1</sup>) and vectors show IVT in exceedance of 250 kg m<sup>-1</sup> s<sup>-1</sup>. The red outline bounds the area satisfying the AR threshold of IVT. (c) Time-latitude plot of the fraction of GEFS members with IVT exceeding 250 kg m<sup>-1</sup> s<sup>-1</sup> making landfall along the west coast of the United States over a 10-day period beginning at 0600 UTC 8 Dec 2016. (d) GEFS-based forecast probabilities of IVT exceeding 250 kg m<sup>-1</sup> s<sup>-1</sup> by latitude for inland points (black dots correspond with bars along y axis) during the 84-h period beginning at 0600 UTC 8 Dec 2016. Gray, blue, and red bars denote >50%, >75%, and >99% chances of exceeding IVT thresholds, respectively. Note the correspondence of the peak of the bar chart with respect to the moisture plume depicted in (c) during the 9–11 Dec 2016 period.

conditions. The bars along the y axis of Fig. 5d indicate the probabilities for AR threshold conditions to occur within an 84-h window at each latitude for inland points (black dots) and can also be used to identify whether moisture will be directed inland along preferential pathways. Figures 5a, 5c, and 5d are accessible at the Scripps Institution of Oceanography's Center for Western Weather and Water Extremes (<http://cw3e.ucsd.edu/>), and Fig. 5b is accessible at the NOAA Western Regional Headquarters Ensemble Graphics page (<http://ssd.wrh.noaa.gov/naefs/?type=ivt>).

The example provided in Fig. 5 was verified at 1200 UTC 11 December 2016 and included an avalanche fatality resulting from substantial new snow falling upon an antecedent weak snowpack. This fatality was observed near Lake Tahoe in western Nevada on 10 December 2016, where intense precipitation associated with the landfalling AR produced 100 mm of new SWE in 36 h. According to the Sierra Avalanche Center (<http://www.sierraavalanchecenter.org>), the avalanche was triggered by a skier and initially failed on a wind

slab that formed during the storm but stepped down to the weak, faceted layer that formed during an anomalously dry November. This unfortunate outcome provides evidence in support of our hypothesis that heavy to extreme precipitation and loading of antecedent shallow and weak snowpacks by ARs favors avalanche occurrence and provides compelling rationale for continuing examination of this hypothesis.

#### f. Precipitation and snowpack loading

Precipitation intensity and total loading of the snowpack are critical components leading to snowpack failure and avalanche formation (Atwater 1954; Schweizer et al. 2003). We use maximum daily precipitation percentile as a proxy for daily loading rate. We also use maximum 1- and 2-day increases in SWE to further examine snowpack loading, as rapid loading promotes snowpack instability since weak layers in the snowpack cannot gain sufficient strength (Schweizer et al. 2003). The use of SNOTEL station data is constrained by gauge undercatch, site locations that likely underestimate the total loading in avalanche start zones, and that station data provide no information regarding snowpack stratigraphy or the presence of weak layers. Detailed snowpit information or avalanche crown profiles were rarely available. Thus, SNOTEL stations represent the best standardized information, available across the wUS, to estimate snowpack loading in the absence of direct precipitation and snowpack measurements. The lack of sufficiently detailed incident reports in many cases precluded us from stratifying SNOTEL stations by elevations that were nearest to the fatality location. No substantial changes in the results occurred by reducing the SNOTEL search radius down to  $0.25^\circ$  from  $0.5^\circ$ .

Our results demonstrate that the avalanche fatalities during AR conditions frequently occurred during heavy ( $>85$ th percentile) to extreme ( $>95$ th percentile) precipitation events (Figs. 6a–i). On average, the median percentile exceeded during avalanche incidents was the 89th, and all states with the exception of Oregon had avalanche events meeting the 99th percentile. The average median  $\Delta$ SWE for all events was 46 mm but varied widely by state and by event (Figs. 7a–i). A common rule of thumb in the wUS assumes ratios of new snow density to range between 70 (continental) and  $120 \text{ kg m}^{-3}$  (coastal), in which case 38–66 cm of new snow would be observed on average (Armstrong and Armstrong 1987). In most cases, the observed  $\Delta$ SWE values are consistent with exceeding the increased avalanche hazard threshold of 30 cm of new snow (Atwater 1954; Perla 1970; Bair 2013). The value of 30 mm of SWE can be considered a conservative estimate, given the uncertainties in SNOTEL data and the extreme variability of snow distribution in complex terrain (Elder et al.

1989; Blöschl 1999; Raleigh and Lundquist 2012). In half of the examined cases, this threshold was met over a 2-day period, and 30% of the cases met this threshold in a single day (Fig. 8). Schweizer et al. (2003) point out that skier-triggered avalanches that lower critical values of new snow, on the order of 10–20 cm, could be observed under unfavorable conditions but depended qualitatively on antecedent snow and weather conditions. Under this assumption and ignoring loading from wind redistribution, sufficient new SWE for skier-triggered avalanches was observed more than half the time in the 1-day SWE increases and over three-quarters of the time in the 2-day SWE increases (Fig. 8). Evaluation of numerous archived accident reports by avalanche centers throughout the western United States indicated that substantial snowpack loading made existing weak layers more susceptible to failure and introduced weak storm snow layers that, upon failure, could step down to cause failure in deeper weak layers. This can result in a much larger and more destructive avalanche due to the increase in mass. These field-based observations and our results further support the notion (see section 4a) that although not all ARs produce fatal avalanches, when AR conditions are forecast, increased situational awareness by avalanche forecasters, ski resort employees, and emergency managers can reduce exposure to resultant avalanche hazards, particularly if antecedent snowpack conditions indicate weakness or poor capability to support substantial new loading. Communicating this awareness to the public is presently being done by many avalanche forecast centers, and our results provide motivation to further increase public recognition regarding potential threats from avalanche hazards during AR events (Doswell et al. 1996).

The greatest median and outlier  $\Delta$ SWE values were found in California (Nevada is excluded because of its small sample size of  $n = 2$ ). This result is consistent with the findings of Ralph and Dettinger (2012) that, as a result of ARs, California receives the greatest 3-day precipitation totals from nonhurricane events in the United States. The lowest  $\Delta$ SWE values were observed in Colorado and Montana. Values of  $\Delta$ SWE exceeding 100 mm occurred less frequently in interior states in accordance with reduced frequencies of AR penetration into the interior wUS (Fig. 1c; Rutz et al. 2014). It would be expected that large  $\Delta$ SWE increases in these inland states require favorable moisture trajectories (Alexander et al. 2015; Rutz et al. 2015) resulting from ideal but rare synoptic conditions. Swales et al. (2016) estimate that up to 70% of Intermountain West extreme precipitation events are associated with synoptic conditions that occur approximately 1.5% of the time.

Occasionally observed negative  $\Delta$ SWE values reflect snowpack depletion, likely due to appreciable melting

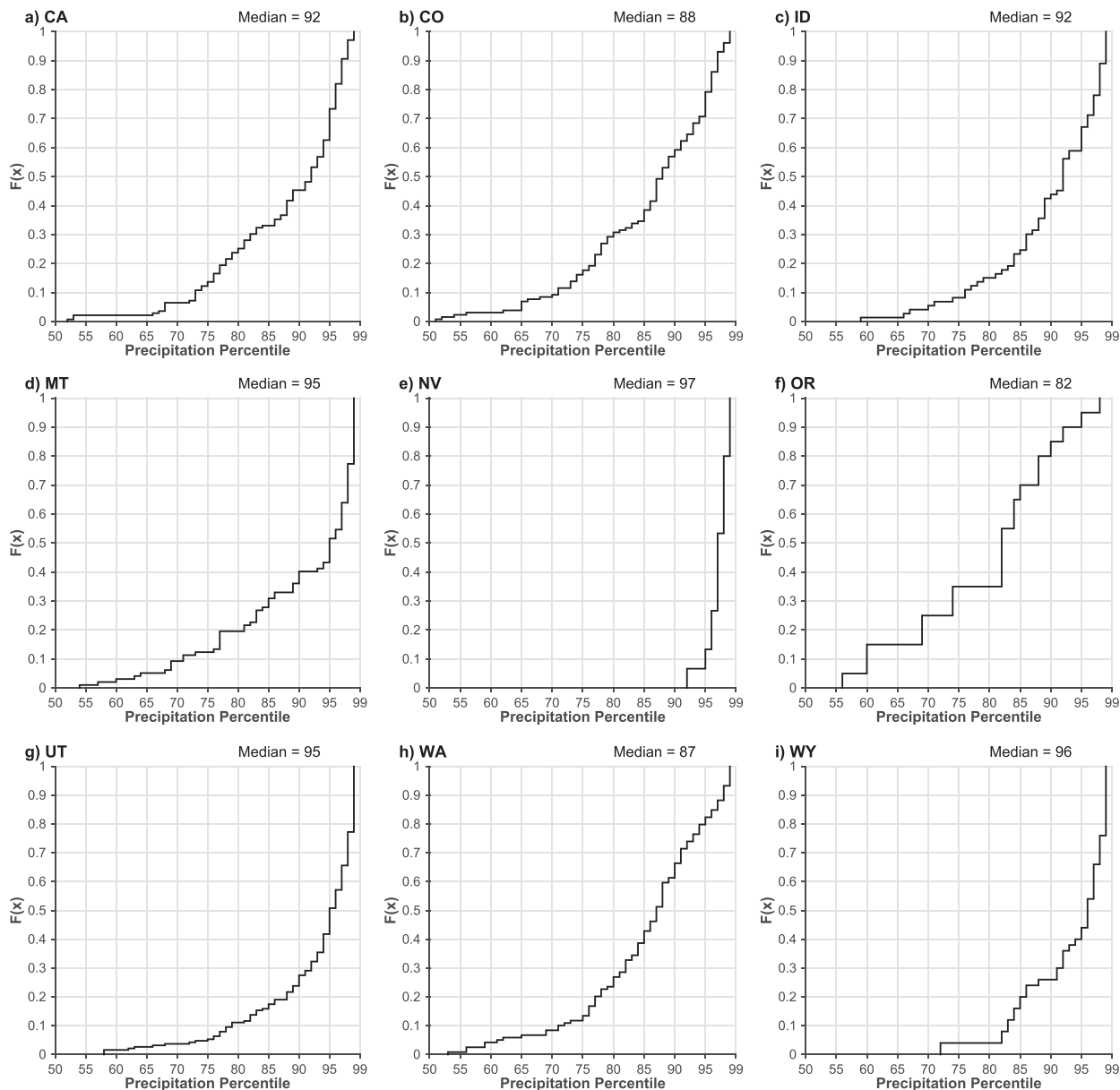


FIG. 6. Cumulative distribution functions of maximum daily cool season precipitation percentile met or exceeded for all stations and all events by state [(a) California, (b) Colorado, (c) Idaho, (d) Montana, (e) Nevada, (f) Oregon, (g) Utah, (h) Washington, and (i) Wyoming] during AR events. Cumulative distribution functions were produced by summing over all SNOTEL stations detected within a  $0.5^\circ$  radius of each fatality by state. Note the negative skew toward heavy (85th) to extreme (99th) percentile precipitation during avalanche fatalities coinciding with AR conditions in nearly all cases. All nonzero cool season precipitation days over each station's period of record were used to estimate the AR event percentiles.

from rain on snow (Marks et al. 1998; Guan et al. 2016). Rain-on-snow events often occur in coastal and inland mountain regions of the wUS during the cool season (McCabe et al. 2007) and promote increases in avalanche activity (Conway and Raymond 1993; Clarke and McClung 1999; Stemberis and Rubin 2011). Rain-on-snow events can trigger immediate increases in avalanche activity via the redistribution of snowpack

stress and delayed avalanche activity once water has penetrated into the snowpack and weakened basal-layer strength (Conway and Raymond 1993). In California, Guan et al. (2016) found that ARs are associated with 50% of rain-on-snow events, which is consistent with the observation that AR storms are typically warmer with a higher melting level compared to other cool season storms (Neiman et al. 2008, 2011;



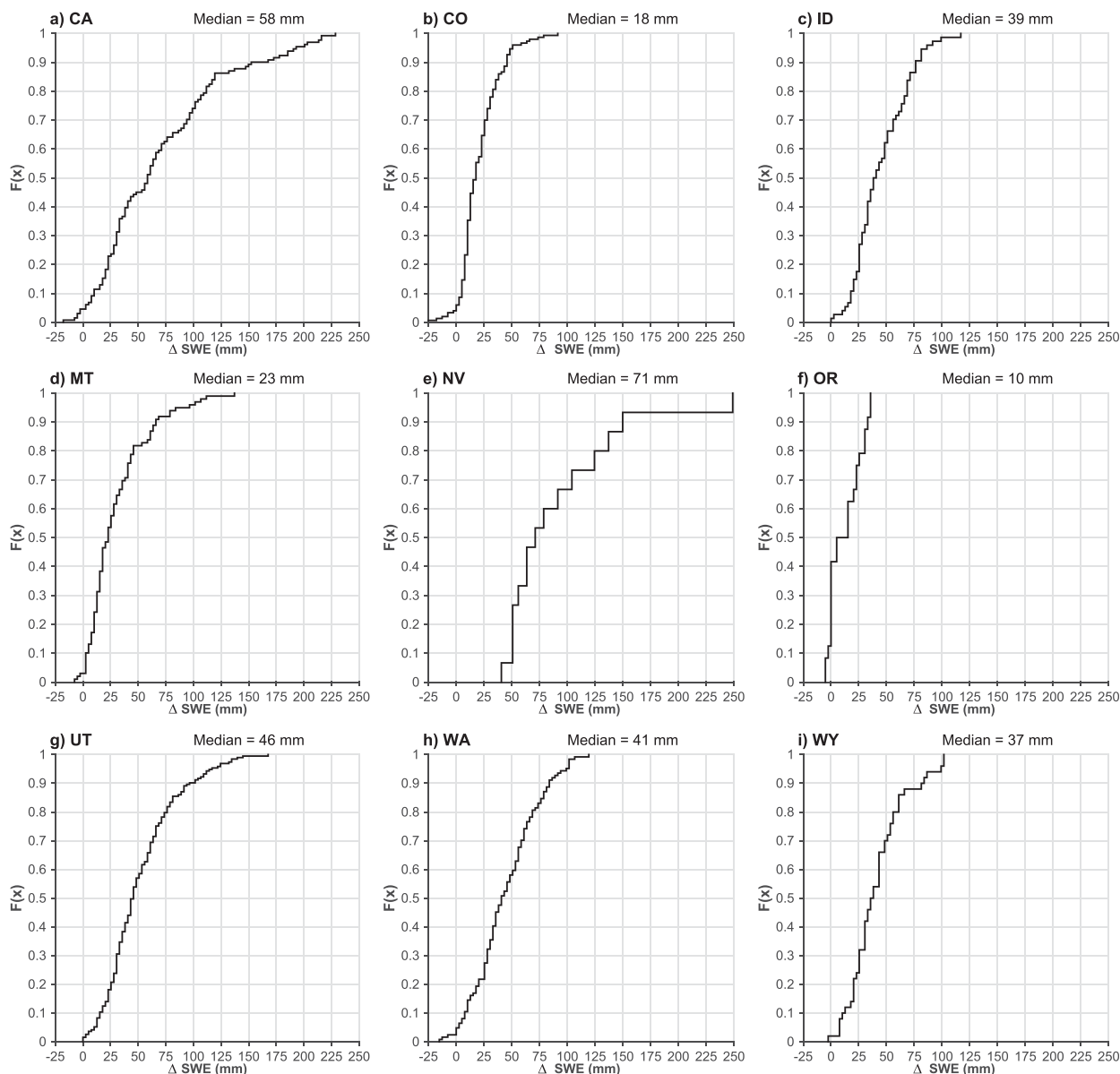


FIG. 7. As in Fig. 6, but for changes in SWE (mm) for all stations and all events by state.

Warner et al. 2012). Based upon existing knowledge, we find it reasonable to assume that AR storms would have a higher likelihood of rain-on-snow occurrence leading to increased avalanche hazard. To fully quantify the frequencies and durations of rain-on-snow events in the wUS, however, the use of hourly precipitation, temperature, and SWE data would be necessary.

Bair (2013) showed surface air temperature changes to be poor predictors of avalanche occurrence. Our investigation found no consistent relationships between surface temperature trends. However, maximum daily increases in 700-hPa air temperatures averaged 4.1 K

(Fig. 9), consistent with quasigeostrophic warm air advection, latent heat release, and upward vertical motion driving enhanced precipitation rates. This finding is consistent with the presence of ridging over the southwestern United States (Fig. 3; Swales et al. 2016) and the fact that atmospheric rivers are associated with the warm sector of cyclones (Ralph et al. 2004).

## 5. Conclusions

Through an examination of archived avalanche fatality incident reports, atmospheric reanalysis products, station data, established snow avalanche climates of the

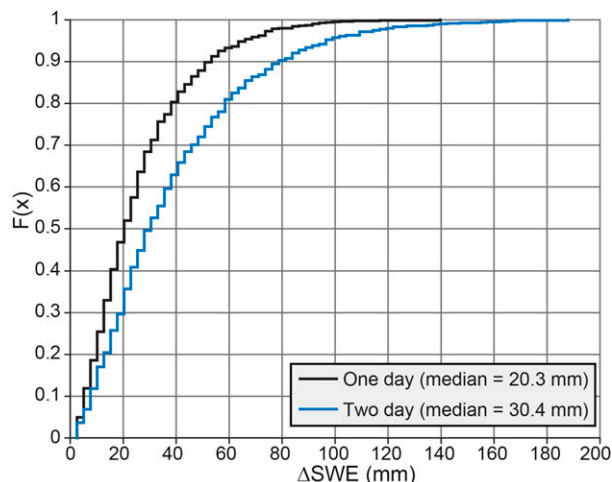


FIG. 8. Cumulative distribution function of max observed 1-day (black) and 2-day (blue) SWE increases (mm) for all stations and all events.

conterminous western US (wUS), and an atmospheric river (AR) catalog, we have shown the following:

- AR conditions were present during 31% of avalanche fatalities in the wUS.
- Our results are consistent with previously established snow avalanche climates and AR-derived cool season precipitation percentages in the wUS. Coastal regions experience the highest percentage of fatalities during ARs, followed in decreasing order by intermountain and continental regions.
- The ratio of fatalities during AR conditions to total number of AR days increased with distance from the coast.
- Observed heavy to extreme precipitation (85th–99th percentile) coincides with AR fatalities.

- Observed SWE increases during AR fatalities often exceeded the critical threshold of 30 mm SWE for avalanche activity over a multiday period, and over both 1-day (30%) and 2-day periods (50%), indicating rapid loading of the snowpack.
- Preferential pathways for inland moisture transport identified by Rutz et al. (2015) and Swales et al. (2016) are consistent with composite analyses of fatalities during AR events in the Intermountain West. Forecasters aware of this relationship may be able to act with additional confidence at times when AR conditions are expected.

This work is a pilot study that demonstrates a possible linkage between ARs and deadly avalanches in the wUS. Continuing research is necessary to improve physical linkages between snowpack stability, loading, and failure during AR events. A more complete analysis to make a concrete linkage was not possible because of the lack of detailed and readily available snowpack and incident information (i.e., stratigraphy and human decision-making processes), limited weather observations, and small sample size of fatalities. Ongoing work seeks to address these limitations by evaluating archived advisories from avalanche centers, conducting interviews with involved parties when possible, and obtaining more meteorological and snowpack data. Our study provides motivation for additional examinations of snow avalanche data with meteorological conditions and preexisting snowpack conditions that favor snowpack instability upon subsequent loading. Detailed information on whether failures occurred on persistent or nonpersistent layers (i.e., storm snow) may be limited to ski resorts (Bair 2013; Marienthal et al. 2015) and even when using all available data, the crystal type of the failure layer is often unknown

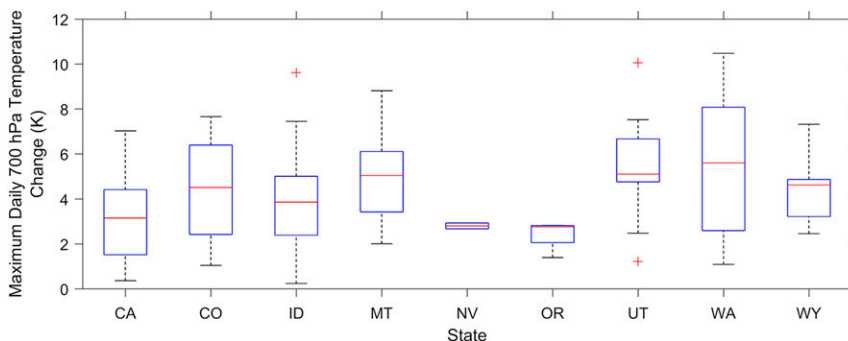


FIG. 9. Box plots grouped by state (from left to right: California, Colorado, Idaho, Montana, Nevada, Oregon, Utah, Washington, and Wyoming) of maximum daily 700-hPa temperature change (K) using the nine nearest NARR grid points to each incident, equivalent to a 0.75° radius. Boxes are drawn about the interquartile range, red lines represent the median values, whiskers extend to  $\pm 2.7\sigma$ , and plus signs represent outliers. The 5-day period covering the incident day and the 4 days prior was considered.

(Bair et al. 2012). Thus, we recommend widespread field efforts to better understand how AR-type storms influence failure mechanisms in storm snow or promote deeper failures on persistent weak layers. Ideally, these studies would combine process-based approaches linking meteorological data, field observations of snowpack stratigraphy and failure, and snowpack-modeling approaches such as SNOWPACK (Bartelt and Lehning 2002) that are suitable for avalanche forecasting (Hirashima et al. 2008). We recommend that during future avalanche fatality evaluations, more detailed information is collected whenever possible to improve subsequent objective analyses, particularly in regards to failure crystal form (Bair et al. 2012), snowpack dynamics, and nonweather (i.e., human) factors. Last, our findings suggest that an increased emphasis on model forecasts of intense water vapor transport and the preferred corridors of inland-penetrating ARs be incorporated into avalanche forecast paradigms to improve assessment of potential avalanche hazards. This may be accomplished through the use of recently developed tools discussed herein and described by Ralph et al. (2013b) and Cordeira et al. (2017).

*Acknowledgments.* Benjamin Hatchett was supported by the Desert Research Institute postdoctoral research funds and a graduate research grant from the American Avalanche Association. Anna Patterson is thanked for cartographic and graphic design suggestions on Fig. 1c. We thank two anonymous reviewers whose critiques and insights improved this manuscript and Jason Cordeira of Plymouth State University who also provided helpful comments.

#### REFERENCES

- Alexander, M. A., J. D. Scott, D. Swales, M. Hughes, K. Mahoney, and C. S. Smith, 2015: Moisture pathways into the U.S. Intermountain West associated with heavy winter precipitation events. *J. Hydrometeorol.*, **16**, 1184–1206, doi:10.1175/JHM-D-14-0139.1.
- Armstrong, R. L., and B. Armstrong, 1987: Snow and avalanche climates of the western United States: A comparison of coastal, intermountain and continental conditions. *IAHS Publ.*, **162**, 281–294.
- Atkins, D., 2007: United States avalanche fatalities. Avalance.org, accessed October 2015. [Available online at <http://www.avalanche.org/accidents.php>.]
- Atwater, M. M., 1954: Snow avalanches. *Sci. Amer.*, **190**, 26–31, doi:10.1038/scientificamerican0154-26.
- Bair, E. H., 2013: Forecasting artificially-triggered avalanches in storm snow at a large ski area. *Cold Reg. Sci. Technol.*, **85**, 261–269, doi:10.1016/j.coldregions.2012.10.003.
- , R. Simenhois, K. Birkeland, and J. Dozier, 2012: A field study on failure of storm snow slab avalanches. *Cold Reg. Sci. Technol.*, **79–80**, 20–28, doi:10.1016/j.coldregions.2012.02.007.
- Bao, J. W., S. A. Michelson, P. J. Neiman, F. M. Ralph, and J. M. Wilczak, 2006: Interpretation of enhanced integrated water vapor bands associated with extratropical cyclones: Their formation and connection to tropical moisture. *Mon. Wea. Rev.*, **134**, 1063–1080, doi:10.1175/MWR3123.1.
- Bartelt, P., and M. Lehning, 2002: A physical SNOWPACK model for the Swiss avalanche warning: Part I: Numerical model. *Cold Reg. Sci. Technol.*, **35**, 123–145, doi:10.1016/S0165-232X(02)00074-5.
- Birkeland, K. W., and C. J. Mock, 1996: Atmospheric circulation patterns associated with heavy snowfall events, Bridger Bowl, Montana, U.S.A. *Mt. Res. Dev.*, **16**, 281–286, doi:10.2307/3673951.
- , —, and J. J. Shinker, 2001: Avalanche extremes and atmospheric circulation patterns. *Ann. Glaciol.*, **32**, 135–140, doi:10.3189/172756401781819030.
- Blackford, J. R., 2007: Sintering and microstructure of ice: A review. *J. Phys. D Appl. Phys.*, **40**, R355–R385, doi:10.1088/0022-3727/40/21/R02.
- Blöschl, G., 1999: Scaling issues in snow hydrology. *Hydrol. Processes*, **13**, 2149–2175, doi:10.1002/(SICI)1099-1085(199910)13:14/15<2149::AID-HYP847>3.0.CO;2-8.
- Clarke, J., and D. McClung, 1999: Full-depth avalanche occurrences caused by snow gliding, Coquihalla, British Columbia, Canada. *J. Glaciol.*, **45**, 539–546, doi:10.1017/S0022143000001404.
- Colorado Avalanche Information Center, 2015: Colorado avalanche incident archive. Accessed October 2015. [Available online at <http://avalanche.state.co.us/accidents/us/>.]
- Conway, H., and C. F. Raymond, 1993: Snow stability during rain. *J. Glaciol.*, **39**, 635–642, doi:10.1017/S0022143000016531.
- Cordeira, J., F. M. Ralph, A. Martin, N. Gaggini, R. Spackman, P. Neiman, J. Rutz, and R. Pierce, 2017: Forecasting atmospheric rivers during CalWater 2015. *Bull. Amer. Meteor. Soc.*, **98**, 449–459, doi: 10.1175/BAMS-D-15-00245.1.
- Dettinger, M. D., F. M. Ralph, T. Das, P. J. Neiman, and D. R. Cayan, 2011: Atmospheric rivers, floods, and the water resources of California. *Water*, **3**, 445–478, doi:10.3390/w3020445.
- Doswell, C. A., III, H. E. Brooks, and R. A. Maddox, 1996: Flash flood forecasting: An ingredients-based methodology. *Wea. Forecasting*, **11**, 560–581, doi:10.1175/1520-0434(1996)011<0560:FFFAIB>2.0.CO;2.
- Elder, K., J. Dozier, and J. Michaelsen, 1989: Spatial and temporal variation of net snow accumulation in a small alpine watershed, Emerald Lake basin, Sierra Nevada, California, U.S.A. *Ann. Glaciol.*, **13**, 56–63, doi:10.1017/S0260305500007643.
- Esteban, P., P. D. Jones, J. Martín-Vide, and M. Mases, 2005: Atmospheric circulation patterns related to heavy snowfall days in Andorra, Pyrenees. *Int. J. Climatol.*, **25**, 319–329, doi:10.1002/joc.1103.
- Fredston, J., and D. Fesler, 2011: *Snow Sense*. Alaska Mountain Safety Center, 132 pp.
- Guan, B., D. E. Waliser, F. M. Ralph, E. J. Fetzer, and P. J. Neiman, 2016: Hydrometeorological characteristics of rain-on-snow events associated with atmospheric rivers. *Geophys. Res. Lett.*, **43**, 2964–2973, doi:10.1002/2016GL067978.
- Hansen, C. S., and S. J. Underwood, 2012: Synoptic-scale weather patterns and large slab avalanches at Mt. Shasta, California. *Northwest Sci.*, **86**, 329–341, doi:10.3955/046.086.0408.
- Hirashima, H., K. Nishimura, S. Yamaguchi, A. Sato, and M. Lehning, 2008: Avalanche forecasting in a heavy snowfall area using the SNOWPACK model. *Cold Reg. Sci. Technol.*, **51**, 191–203, doi:10.1016/j.coldregions.2007.05.013.
- Joseph, P., J. Eischeid, and R. Pyle, 1994: Interannual variability of the onset of the Indian summer monsoon and its association



- with atmospheric features, El Niño, and sea surface temperature anomalies. *J. Climate*, **7**, 81–105, doi:[10.1175/1520-0442\(1994\)007<0081:IVOTOO>2.0.CO;2](https://doi.org/10.1175/1520-0442(1994)007<0081:IVOTOO>2.0.CO;2).
- Kalnay, E., and Coauthors, 1996: The NCEP/NCAR 40-Year Reanalysis Project. *Bull. Amer. Meteor. Soc.*, **77**, 437–471, doi:[10.1175/1520-0477\(1996\)077<0437:TNYRP>2.0.CO;2](https://doi.org/10.1175/1520-0477(1996)077<0437:TNYRP>2.0.CO;2).
- Kapnick, S., and A. Hall, 2012: Causes of recent changes in western North American snowpack. *Climate Dyn.*, **38**, 1885–1899, doi:[10.1007/s00382-011-1089-y](https://doi.org/10.1007/s00382-011-1089-y).
- Krasting, J. P., A. J. Broccoli, K. W. Dixon, and J. R. Lanzante, 2013: Future changes in Northern Hemisphere snowfall. *J. Climate*, **26**, 7813–7828, doi:[10.1175/JCLI-D-12-00832.1](https://doi.org/10.1175/JCLI-D-12-00832.1).
- LaChapelle, E., 1980: Fundamental processes in conventional avalanche forecasting. *J. Glaciol.*, **26**, 75–84, doi:[10.1017/S0022143000010601](https://doi.org/10.1017/S0022143000010601).
- Lavers, D. A., F. Pappenberger, and E. Zsoter, 2014: Extending medium-range predictability of extreme hydrological events in Europe. *Nat. Commun.*, **5**, 5382, doi:[10.1038/ncomms6382](https://doi.org/10.1038/ncomms6382).
- , F. M. Ralph, D. E. Waliser, A. Gershunov, and M. D. Dettinger, 2015: Climate change intensification of horizontal water vapor transport in CMIP5. *Geophys. Res. Lett.*, **42**, 5617–5625, doi:[10.1002/2015GL064672](https://doi.org/10.1002/2015GL064672).
- , D. E. Waliser, F. M. Ralph, and M. D. Dettinger, 2016: Predictability of horizontal water vapor transport relative to precipitation: Enhancing situational awareness for forecasting western U.S. extreme precipitation and flooding. *Geophys. Res. Lett.*, **43**, 2275–2282, doi:[10.1002/2016GL067765](https://doi.org/10.1002/2016GL067765).
- Leung, L. R., and Y. Qian, 2009: Atmospheric rivers induced heavy precipitation and flooding in the western U.S. simulated by the WRF regional climate model. *Geophys. Res. Lett.*, **36**, L03820, doi:[10.1029/2008GL036445](https://doi.org/10.1029/2008GL036445).
- Marienthal, A., J. Hendrikx, K. Birkeland, and K. M. Irvine, 2015: Meteorological variables to aid forecasting deep slab avalanches on persistent weak layers. *Cold Reg. Sci. Technol.*, **120**, 227–236, doi:[10.1016/j.coldregions.2015.08.007](https://doi.org/10.1016/j.coldregions.2015.08.007).
- Marks, D., J. Kimball, D. Tingey, and T. Link, 1998: The sensitivity of snowmelt processes to climate conditions and forest cover during rain-on-snow: A case study of the 1996 Pacific Northwest flood. *Hydrol. Processes*, **12**, 1569–1587, doi:[10.1002/\(SICI\)1099-1085\(199808/09\)12:10<1569::AID-HYP682>3.0.CO;2-L](https://doi.org/10.1002/(SICI)1099-1085(199808/09)12:10<1569::AID-HYP682>3.0.CO;2-L).
- Mass, C., and D. Portman, 1989: Major volcanic eruptions and climate: A critical evaluation. *J. Climate*, **2**, 566–593, doi:[10.1175/1520-0442\(1989\)002<0566:MVEACA>2.0.CO;2](https://doi.org/10.1175/1520-0442(1989)002<0566:MVEACA>2.0.CO;2).
- McCabe, G. J., M. P. Clark, and L. E. Hay, 2007: Rain-on-snow events in the western United States. *Bull. Amer. Meteor. Soc.*, **88**, 319–328, doi:[10.1175/BAMS-88-3-319](https://doi.org/10.1175/BAMS-88-3-319).
- McClung, D. M., 1981: Fracture mechanical models of dry slab avalanche release. *J. Geophys. Res.*, **86**, 10783–10790, doi:[10.1029/JB086iB11p10783](https://doi.org/10.1029/JB086iB11p10783).
- , 2002: The elements of applied avalanche forecasting, Part I: The human issues. *Nat. Hazards*, **26**, 111–129, doi:[10.1023/A:1015665432221](https://doi.org/10.1023/A:1015665432221).
- Meek, D. W., and J. L. Hatfield, 1994: Data quality checking for single station meteorological databases. *Agric. For. Meteorol.*, **69**, 85–109, doi:[10.1016/0168-1923\(94\)90083-3](https://doi.org/10.1016/0168-1923(94)90083-3).
- Mesinger, F., and Coauthors, 2006: North American Regional Reanalysis. *Bull. Amer. Meteor. Soc.*, **87**, 343–360, doi:[10.1175/BAMS-87-3-343](https://doi.org/10.1175/BAMS-87-3-343).
- Mock, C. J., and K. W. Birkeland, 2000: Snow avalanche climatology of the western United States mountain ranges. *Bull. Amer. Meteor. Soc.*, **81**, 2367–2392, doi:[10.1175/1520-0477\(2000\)081<2367:SACOTW>2.3.CO;2](https://doi.org/10.1175/1520-0477(2000)081<2367:SACOTW>2.3.CO;2).
- Mundhenk, B. D., E. A. Barnes, E. D. Maloney, and K. M. Nardi, 2016: Modulation of atmospheric rivers near Alaska and the U.S. West Coast by northeast Pacific height anomalies. *J. Geophys. Res. Atmos.*, **121**, 12751–12756, doi:[10.1002/2016JD025350](https://doi.org/10.1002/2016JD025350).
- Muntán, E., C. García, P. Oller, G. Martí, A. García, and E. Gutiérrez, 2009: Reconstructing snow avalanches in the southeastern Pyrenees. *Nat. Hazards Earth Syst. Sci.*, **9**, 1599–1612, doi:[10.5194/nhess-9-1599-2009](https://doi.org/10.5194/nhess-9-1599-2009).
- Narita, H., 1980: Mechanical behavior and structure of snow under uniaxial tensile stress. *J. Glaciol.*, **26**, 275–282, doi:[10.1017/S0022143000010819](https://doi.org/10.1017/S0022143000010819).
- National Research Council, 1990: *Snow Avalanche Hazards and Mitigation in the United States*. National Academies Press, 84 pp.
- Neiman, P. J., F. M. Ralph, G. A. Wick, J. D. Lundquist, and M. D. Dettinger, 2008: Meteorological characteristics and overland precipitation impacts of atmospheric rivers affecting the West Coast of North America based on eight years of SSM/I satellite observations. *J. Hydrometeorol.*, **9**, 22–47, doi:[10.1175/2007JHM855.1](https://doi.org/10.1175/2007JHM855.1).
- , L. J. Schick, F. M. Ralph, M. Hughes, and G. A. Wick, 2011: Flooding in western Washington: The connection to atmospheric rivers. *J. Hydrometeorol.*, **12**, 1337–1358, doi:[10.1175/2011JHM1358.1](https://doi.org/10.1175/2011JHM1358.1).
- Perla, R. I., 1970: On contributory factors in avalanche hazard evaluation. *Can. Geotech. J.*, **7**, 414–419, doi:[10.1139/t70-053](https://doi.org/10.1139/t70-053).
- Polade, S. D., D. W. Pierce, D. R. Cayan, A. Gershunov, and M. D. Dettinger, 2014: The key role of dry days in changing regional climate and precipitation regimes. *Nat. Sci. Rep.*, **4**, 4364, doi:[10.1038/srep04364](https://doi.org/10.1038/srep04364).
- Raleigh, M. S., and J. D. Lundquist, 2012: Comparing and combining SWE estimates from the SNOW-17 model using PRISM and SWE reconstruction. *Water Resour. Res.*, **48**, W01506, doi:[10.1029/2011WR010542](https://doi.org/10.1029/2011WR010542).
- Ralph, F. M., and M. D. Dettinger, 2012: Historical and national perspectives on extreme West Coast precipitation associated with atmospheric rivers during December 2010. *Bull. Amer. Meteor. Soc.*, **93**, 783–790, doi:[10.1175/BAMS-D-11-00188.1](https://doi.org/10.1175/BAMS-D-11-00188.1).
- , P. J. Neiman, and G. A. Wick, 2004: Satellite and CALJET aircraft observations of atmospheric rivers over the eastern North Pacific Ocean during the winter of 1997/98. *Mon. Wea. Rev.*, **132**, 1721–1745, doi:[10.1175/1520-0493\(2004\)132<1721:SACAOO>2.0.CO;2](https://doi.org/10.1175/1520-0493(2004)132<1721:SACAOO>2.0.CO;2).
- , —, —, S. I. Gutman, M. D. Dettinger, D. R. Cayan, and A. B. White, 2006: Flooding on California's Russian River: Role of atmospheric rivers. *Geophys. Res. Lett.*, **33**, L13801, doi:[10.1029/2006GL026689](https://doi.org/10.1029/2006GL026689).
- , T. Coleman, P. J. Neiman, R. J. Zamora, and M. D. Dettinger, 2013a: Observed impacts of duration and seasonality of atmospheric-river landfalls on soil moisture and runoff in coastal Northern California. *J. Hydrometeorol.*, **14**, 443–459, doi:[10.1175/JHM-D-12-076.1](https://doi.org/10.1175/JHM-D-12-076.1).
- , and Coauthors, 2013b: The emergence of weather-focused test beds linking research and forecasting operations. *Bull. Amer. Meteor. Soc.*, **94**, 1187–1211, doi:[10.1175/BAMS-D-12-00080.1](https://doi.org/10.1175/BAMS-D-12-00080.1).
- Rutz, J. J., W. J. Steenburgh, and F. M. Ralph, 2014: Climatological characteristics of cool season atmospheric rivers and their inland penetration over the western United States. *Mon. Wea. Rev.*, **142**, 905–921, doi:[10.1175/MWR-D-13-00168.1](https://doi.org/10.1175/MWR-D-13-00168.1).
- , —, and —, 2015: The inland penetration of atmospheric rivers over western North America: A Lagrangian analysis. *Mon. Wea. Rev.*, **143**, 1924–1944, doi:[10.1175/MWR-D-14-00288.1](https://doi.org/10.1175/MWR-D-14-00288.1).

- Schweizer, J., and J. B. Jamieson, 2001: Snow cover properties for skier triggering of avalanches. *Cold Reg. Sci. Technol.*, **33**, 207–221, doi:[10.1016/S0165-232X\(01\)00039-8](https://doi.org/10.1016/S0165-232X(01)00039-8).
- , and —, 2003: Snowpack properties for snow profile interpretation. *Cold Reg. Sci. Technol.*, **37**, 233–241, doi:[10.1016/S0165-232X\(03\)00067-3](https://doi.org/10.1016/S0165-232X(03)00067-3).
- , —, and M. Schneebeli, 2003: Snow avalanche formation. *Rev. Geophys.*, **41**, 1016, doi:[10.1029/2002RG000123](https://doi.org/10.1029/2002RG000123).
- , K. Kronholm, J. B. Jamieson, and K. W. Birkeland, 2008: Review of spatial variability of snowpack properties and its importance for avalanche formation. *Cold Reg. Sci. Technol.*, **51**, 253–272, doi:[10.1016/j.coldregions.2007.04.009](https://doi.org/10.1016/j.coldregions.2007.04.009).
- Serreze, M. C., M. P. Clark, and A. Frei, 2001: Characteristics of large snowfall events in the montane western United States as examined using snowpack telemetry (SNOTEL) data. *Water Resour. Res.*, **37**, 675–688, doi:[10.1029/2000WR900307](https://doi.org/10.1029/2000WR900307).
- Stimberis, J., and C. M. Rubin, 2011: Glide avalanche response to an extreme rain-on-snow event, Snoqualmie Pass, Washington, USA. *J. Glaciol.*, **57**, 468–474, doi:[10.3189/002214311796905686](https://doi.org/10.3189/002214311796905686).
- Swales, D., M. Alexander, and M. Hughes, 2016: Examining moisture pathways and extreme precipitation in the U.S. Intermountain West using self-organizing maps. *Geophys. Res. Lett.*, **43**, 1727–1735, doi:[10.1002/2015GL067478](https://doi.org/10.1002/2015GL067478).
- Warner, M. D., C. F. Mass, and E. P. Salathé, 2012: Wintertime extreme precipitation events along the Pacific Northwest coast: Climatology and synoptic evolution. *Mon. Wea. Rev.*, **140**, 2021–2043, doi:[10.1175/MWR-D-11-00197.1](https://doi.org/10.1175/MWR-D-11-00197.1).
- Zhu, Y., and R. E. Newell, 1998: A proposed algorithm for moisture fluxes from atmospheric rivers. *Mon. Wea. Rev.*, **126**, 725–735, doi:[10.1175/1520-0493\(1998\)126<0725:APAFMF>2.0.CO;2](https://doi.org/10.1175/1520-0493(1998)126<0725:APAFMF>2.0.CO;2).